

# PREDICTING THE AEROACOUSTIC BEHAVIOUR OF AIRCRAFT AIR-DISTRIBUTION SYSTEM BY USING NEURO-FUZZY LOCAL MODEL NETWORKS

Syed Fawad Bokhari, Otto von Estorff

[bokhari@tuhh.de](mailto:bokhari@tuhh.de), [estorff@tuhh.de](mailto:estorff@tuhh.de)

*Institute of Modelling and Computation  
Hamburg University of Technology (TUHH)*

**Abstract** Early design phase of an aircraft requires reducing a flow noise in an air-distribution system. This necessitates predicting an aeroacoustic behaviour of its components, which can either be done by employing extensive numerical simulations or by using experimental data. This paper deals with the latter and a systematic and an efficient method of utilizing the experimental data for an estimation of empirical models is presented. A single-hole orifice has been taken as a representative example, for a component of an air-distribution system, to demonstrate that same approach can be used to model other components. The presented approach uses Neuro-Fuzzy based Local Models, which have been estimated at different geometries and flow conditions, and a network of these Local Neuro-Fuzzy Models, known as a Local Model Network, has been used to cover the complete set of conditions. Dimensional analysis of the problem, presented here, reveals that the aeroacoustic spectrum depends on a dimensionless number that is defined by the sound power, its frequency, the geometry of a component and the density of the fluid. Two empirical models have been developed by using this approach. The inputs to the models are the geometric parameters of the orifice and the flow conditions. Both models have different accuracies and complexities, where the first model can predict the newly found dimensionless number up to Helmholtz number of 5.83 while the second model consists of only one local model and the prediction horizon reduced to 3.64 .

**Keywords** Aeroacoustic prediction, empirical modelling, Neuro-Fuzzy, Local Model Network, air duct system

## Abbreviations

<i>ANN</i>	Artificial Neural Network
<i>DNS</i>	Direct Numerical Simulation
<i>IATA</i>	International Air Transportation Association
<i>LES</i>	Large Eddy Simulation
<i>LMN</i>	Local Model Network
<i>LOLIMOT</i>	Local Linear Model Tree
<i>PCDN</i>	Power coefficient based dimensionless number
<i>RANS</i>	Reynolds Average Navier-Stokes

<i>RBF</i>	Radial Basis Function
<i>WPR</i>	Worst Performing Regime

## 1 Introduction

Due to comfort reasons, a flow noise in an air-distribution system has become a great concern for an aircraft system designer. Presently, IATA facts and figures for public health preparedness state that for a safe cabin environment, almost 15 to 20 cubic feet of a total air flow supply per minute and per person is required in an economy class [1]. The flow produces an aerodynamically generated sound which can be termed as noise, being unwanted and not comfortable. In this regard, the passenger's demands, for the reduced flow noise, are required to be accounted for in an aircraft cabin design. So far, the noise reduction has been dealt with by using passive techniques (insulation) but a more promising strategy is to modify the structure and the geometry of the system [2, 3]. However, the modifications involve a design optimization that requires iterative evaluations of an aeroacoustic prediction in different parts of the air-distribution system, which is a rather challenging task.

Accurate aeroacoustic behaviour of a complex flow is very difficult to model and to predict [4] since it is generally infeasible to comprehensively and accurately estimate the effects of different dynamic processes playing their role in overall aeroacoustic behaviour [2]. The flow noise of a complex flow involves a non-linear interaction of velocity fluctuations, entropy fluctuations, viscous stresses, and vorticity of the flow passing through the different geometries of the duct system. In addition, the presence of solid boundaries enhances the conversion from flow energy to acoustic energy [2]. So far, different computational methods, e.g. DNS, LES, RANS method, etc., have been used in the process of the aeroacoustic prediction. However, the prediction is a challenge not only due to the time and the hardware resource involved [2, 5] but also due to the insufficient level of a theoretical comprehension about the aeroacoustic phenomena [2, 3]. In particular, Ferdononki [3] has discussed in detail about the fundamental flaws in the basic aeroacoustic theories and asserts that it is very difficult to select an absolutely flawless method.

Hence, the aeroacoustic prediction of an air-distribution system poses a difficult problem for a cabin system designer since it requires undertaking the aeroacoustic evaluation for each geometric modification before finalizing the cabin system specification. In addition, the time and the resource consuming requirements of the computational tools and the insufficiency of knowledge limits the system design process up to a trial and error [2, 6] approach.

In this regard, this paper suggests an alternative to build an empirical model that performs the required task at a design and optimization level. The fundamental idea is to develop nonlinear empirical models for different components of an air-distribution system and to use them for the design optimization. The models of individual components can be modularly combined, each as a simulation block, to simulate an entire duct system. So, the empirical model of an individual component, e.g. model for single-hole orifice, becomes one of a block inside a complete simulation model for a whole duct system. A representative example, namely a single-hole orifice, is considered in order to demonstrate the empirical modelling of a single block, and it can be inferred that the same approach can be applied for other components.

An empirical model results after investigating influences of different independent factors on quantities through pure experimental data. The independent and dependent quantities are also referred as inputs  $\theta$  and outputs  $y$  of an empirical model. The empirical modelling is done in two steps: Firstly, a model structure is finalized that defines a relation between the inputs and the outputs, e.g. the model structure for the single-hole orifice relates that how different flow and geometric conditions relate to an acoustic spectrum. Secondly and finally, the model parameters are identified by using parameter optimization methods [10].

As far as empirical modelling is concerned, recent years have seen numerous developments in nonlinear empirical modelling among which the artificial neural networks and fuzzy systems are the prominent ones [7–14]. A further extension is to use a hybrid approach, where artificial neural networks and fuzzy systems are synergically combined to form the so called Neuro-Fuzzy based Local Model Network [7]. The base is an approach which is referred as a “*divide-and-conquer strategy*” or an “*operating regime approach*” [10, 11]. The approach is implemented by decomposing a complex problem (prediction of a flow noise in an orifice) into a number of sub problems (operating regime) by partitioning an input space or operating points. This leads to a network of sub models or local model(s) that is known as a Local Model Network. Each model is valid in the corresponding operating regime, which is defined by radial basis function based validity functions. The rationale behind is that the behaviour of a sub model is simpler than the

global behaviour of a complex problem, e.g. complex problem of flow noise prediction in a single-hole orifice. In particular, a sub model can easily be identified and solved independently by using the established techniques in a linear system theory [10, 11].

This paper presents empirical modelling for a single-hole orifice, which defines that how a Helmholtz number, a diameter ratio, and a Reynolds number relates to a newly introduced power coefficient based dimensionless number. In this connection, series of experiments have been conducted by using a specially developed experimental environment [6], which allows to take into account different flows and geometric conditions. The measured data have been eventually used to identify the models. The final models, presented here, use the geometric and fluid conditions as inputs and effectively predict the aeroacoustic behaviour of single-hole orifice by yielding an acoustic spectrum.

## 2 Neuro-Fuzzy systems

A Neuro-Fuzzy system is a synergic combination of RBF based Artificial Neural Networks and advanced fuzzy systems that form the basis of Local Model Networks [7–13]. The ANNs and the fuzzy system are essential components that are necessary for the implementation of LMNs.

### 2.1 Artificial Neural Networks

An artificial neural network is inspired by a biological neural network [9], which is a complex interconnection of biological neurons, see figure 30 in appendix. A rather simplified mathematical equivalence of a biological neuron is known as an artificial neuron. An artificial neuron is the fundamental unit of an ANN that can model any complex phenomenon by using the input and output data, e.g. it can model aeroacoustic behaviour of a single-hole orifice.

An artificial neuron, see figure 1, constitutes of a summation function, i.e. performs a summation of all input signals, and an activation function  $f_{ai}$ , e.g. unit step function, sigmoid function, ramp function etc., see figure 32 in appendix.

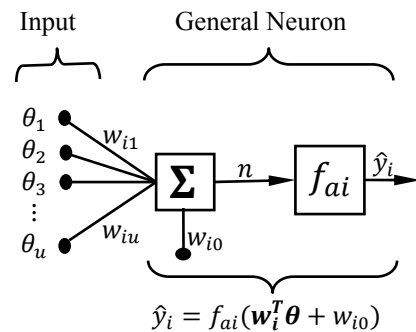


Fig 1 An artificial Neuron, according to [21]

Similar to a biological neuron, a particular  $i^{th}$  neuron receives all the  $u$  number of inputs ( $\theta \in \mathbb{R}^u$ ) that are weighted beforehand by suitable constants  $w_{ij}$ . The summation function adds the weighted inputs ( $w_{ij}u_j$ ) and a bias weight to form a scalar signal, i.e.  $w_i^T \theta + w_{i0}$ . The activation function  $f_{ai}$  processes the scalar signal to produce an activation signal which can be referred as a local output

$$\hat{y}_i = f_{ai}\left(\sum_{j=1}^u w_{ij}u_j + w_{i0}\right) \quad (1)$$

for the neuron of a general ANN [10], see figure 1. Finally, a complete model can constitute more than one artificial neurons, i.e.  $M$  neurons, and predicts the required output, e.g. predicted results of a single-hole orifice.

A variation of an ANN is a RBF network that uses a RBF, e.g. Gaussian function  $\mu$ , as an activation function, see figure 2 and 31. Depending upon the deviation of the input values from the reference value (called as the centre value  $c$  of an RBF), the activation function produces a scalar valued activation signal, whose value lies between 0 and 1, i.e.  $\mu = [0,1]$ . Where, the value of 1 represents no deviation of the input data from the centre value, and 0 indicates that the deviation is more than the reference deviation, [10, 14], i.e. the deviation is more than a particular multiple of the spread of the data  $constant \times [\max(\theta_j) - \min(\theta_j)]$ . Finally, the  $i^{th}$  neuron of an NRBF yields the output

$$\hat{y}_i = w_{i0}\mu_i(\theta, c_i, \sigma_i) \quad (2)$$

by multiplying an activation signal and a bias weight, see figure 2. Where  $c_i \in \mathbb{R}^u$  and  $\sigma_i \in \mathbb{R}^u$ , also known as the premises parameters, are the centre values and the standard deviations for the RBF.

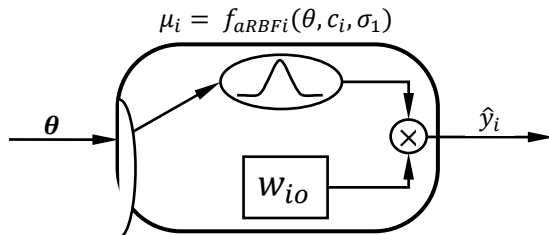


Fig 2 A neuron of radial basis function network

It can be concluded from figure 2 that the weight  $w_{i0}$  of the  $i^{th}$  neuron only contributes significantly to an overall output, when particular discrete values of inputs are within the range of the premises parameters for the corresponding RBF  $\mu_i$ . So if there are particular discrete values of the inputs then a corresponding RBF would significantly influence the predicted final output. Figure 3 shows an example of a multi input and single output

(MISO) system represented by a RBF network that constitutes  $M$  Gaussian functions.

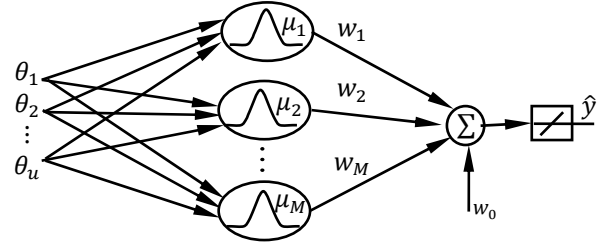


Fig 3 A radial basis function network, according to [10]

## 2.2 Fuzzy system

The artificial neural networks are capable of modelling any given data, i.e. they are universal approximators, but they lack interpretability. Alternatively, fuzzy systems incorporate qualitative expert knowledge (priors physical information and subjective insight). It analyses in terms of variables that take on continuous values between 0 and 1. The fuzzy system uses the expert knowledge in the form of linguistic expressions or rules and linguistic outputs [10, 14] which are then transformed into fuzzy numbers. The rules, which are *if-then* statements, depicts that *if* an antecedent proposition *then* a consequent proposition holds, e.g. *if* the velocity is  $3 \frac{m}{sec}$ , *and if* the diameter ratio is 0.77 *then* the single-hole orifice contributes *less* noise. There is a similarity between the RBF network and the fuzzy system in the sense that the “trueness” of the *if* statement or rule is validated through the fuzzy logic based membership functions  $MSF$  (see figure 3 and 4), which are functionally analogous and similar to the RBF based activation function, e.g. Gaussian function.

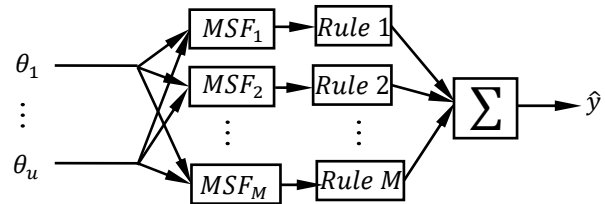


Fig 4 Takagi-Sugano Model for fuzzy systems according to [22]

A further extension of the fuzzy system is a Takagi-Sugeno fuzzy system which, unlike the classical fuzzy system, realizes the output rules as equations (*if* Rule  $i$  *then*  $\hat{y}_i$  is  $f_i(\cdot)$ ), see figures 4 and 5, and finally forms the basis for the Neuro-Fuzzy systems [10, 14]. The Takagi-Sugeno model yields the output

$$\hat{y} = \sum_{i=1}^M \underbrace{(w_{i0} + w_{i1}\theta_1 + \dots + w_{iu}\theta_u)}_{\hat{y}_i} MSF_i \quad (3)$$

by summing all the multiples of the function  $\hat{y}_i$  and corresponding membership function  $MSF_i$ . And similar to the RBF network, the membership function enforces

the significance of a particular function  $\hat{y}_i$ , when the discrete value of the inputs lie within the regime of the  $MSF_i$ , see figure 5.

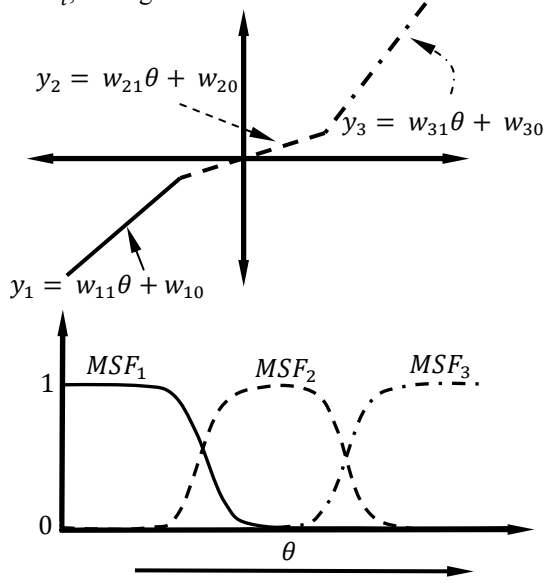


Fig 5 An example of a Takagi-Sugeno Model, according to [9]

### 3 Local Model Network

The Takagi-Sugeno model, eq(3), forms the basis of a Local Model Network. The  $i^{th}$  neuron of a Neuro-Fuzzy based Local Model Network, known as  $i^{th}$  Local Model  $LM_i$ , forms when any function  $f_i$  replaces the weight  $w_{i0}$  of a corresponding neuron inside an RBF network, see figures 2 and 6.

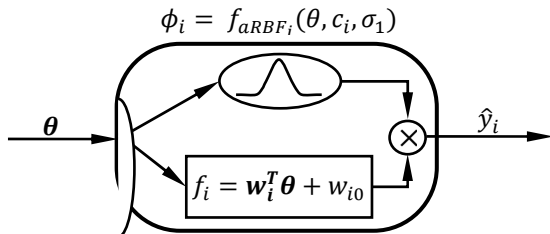


Fig 6 Neuro-Fuzzy Local Model

Where, a particular validity function  $\phi_i$  defines the local validity of the corresponding model, i.e. the validity function  $\phi_i$  restricts the validity of the local model  $LM_i$  in the region defined by  $c_i$  and  $\sigma_i$ . The validity function are chosen as a normalized axis orthogonal Gaussian function, such that

$$\phi_i = \frac{\mu_i(\theta)}{\sum_{j=1}^M \mu_j(\theta)} \quad \text{and} \quad \sum_{i=1}^M \phi_i(\theta) = 1 \quad (4)$$

holds for all of the  $u$ . Thus, the final model for the Neuro-Fuzzy system, e.g. the model for the single-hole orifice, yields the output

$$\hat{y} = \sum_{i=1}^M \frac{(w_{i0} + w_{i1}\theta_1 + \dots + w_{iu}\theta_u)}{LM_i} \phi_i \quad (5)$$

by combining all the  $M$  local models. The final model can be conceived as a network of  $M$  different local models, see figure 7, and called as a Local Model Network. Here,  $M$  different validity function restricts the validity of corresponding models. As an example, a model structure of the Neuro-Fuzzy based Local Model Network for a multi input and single output system, is shown in figure 7.

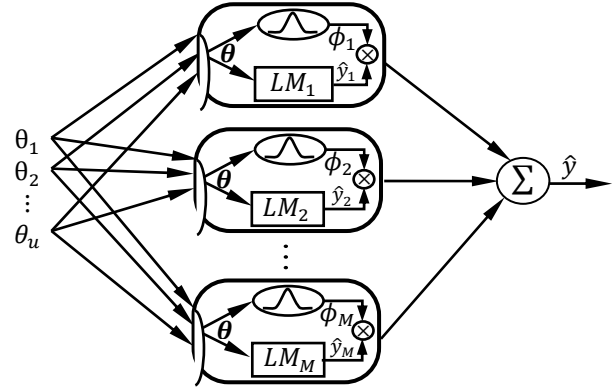


Fig 7 Neuro-Fuzzy based Local Model Network, according to [10]

The crux of a Local Model Network technique is to decompose or partition, a complex problem regime into  $M$  different operating regimes with the help of a "divide and conquer strategy" [11]. Each regime is independently modelled and its region of validity is identified by determining the premises parameters of the corresponding validity function eq(4), [7–13], see figure 8. In this regard, the centre value (mean) and the spread of the data in  $i^{th}$  partition define the premises parameters for the corresponding regime, i.e. they define the  $i^{th}$  validity function for the corresponding local model  $LM_i$ .

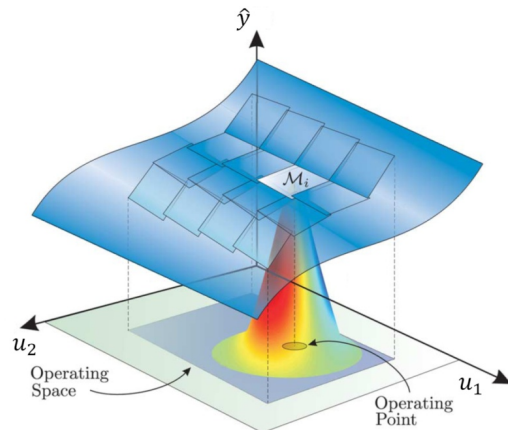


Fig 8 A particular operating regime validated by a corresponding validity function [7]

In this regard, an efficient and widely used decomposition algorithm [10] is to heuristically partition the input space and to develop an independent Local Model for each partition. Initially, the input space is coarsely partitioned, i.e.  $i = M = 1$ , to make one global linear model. Then the  $i^{\text{th}}$  loss function

$$I_i = \sum_{j=1}^N (y_j - \hat{y}_j)^2 \phi_i(c_i, \sigma_i), \quad (6)$$

is calculated and eventually minimized by systematically increasing the partitions until the desired results are obtained. In this regard, a LOLIMOT algorithm that is an axis orthogonal, heuristic and an incremental construction algorithm [10], implements the required decomposition scheme, see figure 9, in the following way:

1. Initialize a single regime, i.e. start with a coarse model of a single partition ( $i = M = 1$ )
  - a. Fit a global linear model, e.g. global linear model for an orifice.
  - b. Find the weights, i.e.  $\mathbf{w}_i^T$  and  $w_{i0}$ , and premises parameters, i.e.  $c_i$  and  $\sigma_i$ .
2. Find the worst performing regime
  - a. Find the loss functions, eq (6), for all the partitions, i.e.  $i = 1, \dots, M$ .
  - b. Find the partition, i.e.  $WPR$ , with the maximum value of loss function, i.e.  $\max([I_1, I_2, \dots, I_i, \dots, I_M])$ .
3. Partition the  $WPR$ , in all dimensions ( $dim = 1, \dots, u$ ).
  - a. Split the  $WPR$ , axis orthogonally, into two, by separately dividing the input space in all the dimensions.
  - b. Find the weights and construct the validity function for the two hyper rectangular halves.
  - c. Find the loss function for all the  $u$  alternatives.
4. Select only the best partition
  - a. Select the best of the  $u$  possibilities.
  - b. Adopt the validity functions and weights of the corresponding partitions.
  - c. The number of partitions is increased by one, i.e.  $M \rightarrow M + 1$ .
5. Test for termination of algorithm
  - a. If the criteria are met, i.e. maximum iteration or minimum acceptable error etc., then stop the algorithm, else go to step 2.

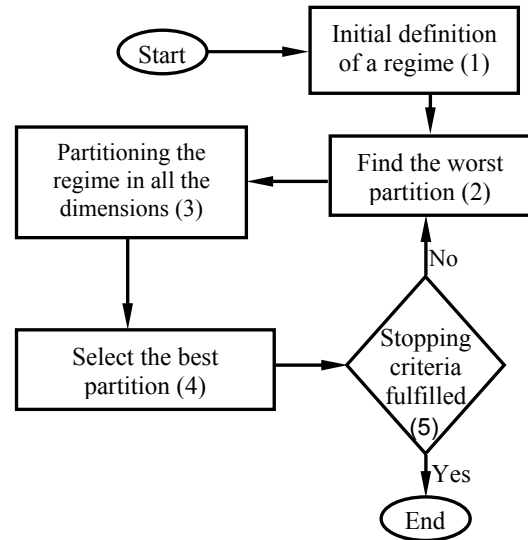


Fig 9 The LOLIMOT algorithm

## 4 Empirical model of a single-hole orifice

In this paper, a single-hole orifice is selected as a representative example to demonstrate that same technique can be used to model their aeroacoustic behaviour. An orifice serves to restrict the flow and helps to regulate it. However, the sudden change in the area causes pressure fluctuations [4] that make it a noise source. Such a source adds its contribution to the existing flow noise of the hollow pipe. The prediction of the additional noise is essentially the acoustic prediction of a single-hole orifice.

The modelling procedure requires the input-output data, which is reproduced at conditions close to those inside an air-distribution system. This is done by producing different flow and geometric conditions at the input cross section of the single-hole orifice. In this regard, a special experimental environment [6], has been used to produce different experimental operating condition (operating points). The experimental environment consists of a setup of hardware and software components, which are essential for the repeatability, see figure 10. A flow is produced by a fan that is regulated by using a controller, throttle, bypass and flow measurement sensor. The regulated flow, still polluted with a fan noise, is passed through series of noise dampers to diminish the fan noise, i.e. only flow noise remains afterwards. The flow is straightened and passed through a long pipe, with a diameter  $D$ , to bring the flow in a steady state condition. A reference part, e.g. a single-hole orifice, is placed afterwards to receive the required flow as an input. An impedance converter, which is a special divergent horn, is placed afterwards at the exit section of the reference part to reduce the sound reflection back into the flow. The flow is allowed to enter a special

reverberating room, which is a special room and made of reflecting and non-parallel walls. Finally, by using the standard DIN ISO 3741, the sound power level of the source has been found out by measuring the sound pressure level in the room.

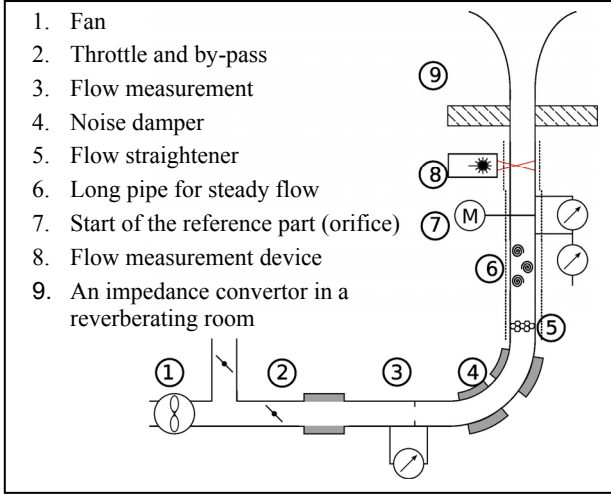


Fig 10 Components of experimental setup

#### 4.1 A single-hole orifice and variable of interest

A single-hole orifice is a circular disc with a hole inside, see figure 11 and is a component of an air-distribution system. An important geometric variable of interest is the internal diameter  $d$  of an orifice. A variation in the diameter influences the flow fluctuations and essentially affects the sound power. The outer diameter of the orifice matches the outer diameter of the pipe in which the orifice has been placed.

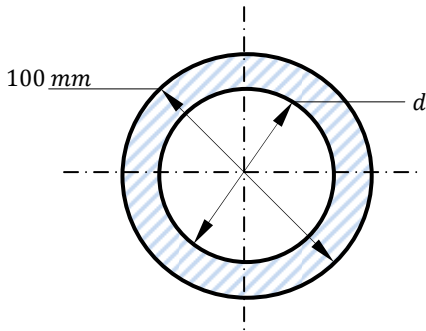


Fig 11 A single-hole orifice

The flow velocity  $v$  at the orifice and the orifice diameter  $d$  decisively affect the sound power and can also be controlled by the experimental environment, i.e. they can be precisely changed to produce different flows and geometric conditions. In addition, the density  $\rho$  and the viscosity  $\mu$  of the fluid also play an important role in an overall fluid behaviour and hence should be included for investigating the aeroacoustics inside the duct system. Finally, the frequency  $f$  must also be incorporated as an

input for the model because the final objective is to predict the spectrum of the sound power  $P$ , such that an intermediate model can be defined as

$$P = f(v, d, \rho, \mu, f). \quad (7)$$

The current paper uses the matrix method [16] for the dimensional analysis [4, 15, 16] of the variables. After some initial re-arrangements the non dimensional quantities have been deduced, which are shown in the table 1.

Table 1: Non-dimensional quantities

Variables of interest	Formula
Reynolds number	$R_e = \frac{\rho d v}{\mu}$
Diameter ratio	$\beta = \frac{d}{D}$
Helmholtz Number	$kD = \frac{fD}{c}$
Power coefficient based number	$PCDN = \frac{P}{\rho d^5 f^3}$

#### 4.2 Power coefficient based dimensionless number

The current paper introduces a new power coefficient based dimensionless acoustic quantity that is referred, here, as a power coefficient based dimensionless number  $PCDN$ , see table 1. Unlike conventional acoustic quantity, i.e. sound power level, the number has an advantage that it eases the empirical modelling process. Since the sound power is used in a logarithmic form, the finalized output variable is suggested as

$$PCDN = 10 \log_{10} \left( \frac{P}{\rho d^5 f^3} \right) \quad (8)$$

or by

$$PCDN = 10 \log_{10} \left( \frac{P}{P_o} \right) + 10 \log_{10} \left( \frac{P_o}{\rho d^5 f^3} \right) \quad (9)$$

where the first term on the right hand side is the standard sound power level in  $dB$  and  $P_o$  is the reference sound power level, i.e.  $10^{-12}$  Watts. So a non dimensional model for power coefficient based dimensionless number

$$PCDN = L_w + 10 \log_{10} \left( \frac{P_o}{\rho d^5 f^3} \right) = f(R_e, \beta, kD), \quad (10)$$

should be found out. Finally the sound power level can be found by using the following

$$L_w = PCDN - 10 \log_{10} \left( \frac{P_o}{\rho d^5 f^3} \right). \quad (11)$$

### 4.3 Operating points and experiments

Series of experiments have been conducted by using both factorial and random based experimental [17, 18] design to ensure the reproducibility and repeatability of the experimental data. In order to apply the LOLIMOT algorithm, all the input combinations are concatenated to form a matrix of operating points (input matrix), which serve as one of the input for the LOLIMOT algorithm, see figure 12.

As a general case there are  $s$  different operating points which are arranged in the form of a matrix  $opPoints \in \mathbb{R}^{s \times u}$ , where each  $b^{th}$  row represents a  $u$  dimensional operating point ( $u$  is the number of columns  $\theta \in \mathbb{R}^u$ ). The operating point represents a unique combination of available discrete values for all the  $u$  variables of interest (input parameters). Where, each  $q^{th}$  column of the  $b^{th}$  operating point

$$b^{th}OpPoint = [\theta_{1(p_1)}, \theta_{2(p_2)} \dots \theta_{q(p_q)}, \dots \theta_{u(p_u)}] \quad (12)$$

represents the  $(p_q)^{th}$  value  $\theta_{q(p_q)}$  of the corresponding input. Here, as an example,  $\theta_{q(p_q)} = \theta_{3(10)}$  denotes the  $10^{th}$  discrete value ( $p_q = 10$ ) of the  $3^{rd}$  input ( $\theta_q = \theta_3$ ). Finally, in the case of a single-hole orifice the  $b^{th}$  operating point becomes

$$b^{th}OpPoint = [\beta_{(p_1)}, Re_{(p_2)}, kD_{(p_3)}]. \quad (13)$$

In addition, a detailed data exploration has revealed the underlying structure for the relation between the power coefficient based dimensionless number and the Helmholtz number. It is clear from figure 18 – 20 that the power law relation

$$PCDN = \alpha (kD)^n \quad (14)$$

holds for the all the measured data. So, an operating point matrix of the following form

$$newB^{th}Row = [\beta_{(p_1)}, Re_{(p_2)}, kD_{(p_3)}^n] \quad (15)$$

can replace eq (13) for further analysis and eq (10) can be finally modified to

$$PCDN = L_w + 10 \log_{10} \left( \frac{P_o}{\rho d^5 f^3} \right) = f(Re, \beta, kD^n), \quad (16)$$

where, further data exploration revealed that the overall best result could be achieved when

$$n = 0.15. \quad (17)$$

In these experiments five different diameter ratios

$$\beta \in \mathbb{R}^5 = [0.38, 0.49, 0.56, 0.68, 0.77]^T,$$

have been taken and 4 different Reynolds numbers ,for each diameter ratio,

$$R_e \in \mathbb{R}^4 = [500 \ 676 \ 852 \ 1030]^T \times 10^2,$$

have been selected. In addition, 19 discrete frequency bands for the Helmholtz number

$$kD \in \mathbb{R}^{19} \text{ corresponding to } = [315 \text{ Hz}, \dots, 20 \text{ kHz}] \in \mathbb{R}^{19},$$

have been considered for the modelling and hence for the experiments. This lead to the final input matrix, made up of operating points, becomes

$$opPoints \in \mathbb{R}^{(5 \times 4 \times 19) \times u = 380 \times 3}.$$

Finally, for each of the operating points, the power coefficient based dimensionless number has been calculated to obtain the corresponding data output vector  $y \in \mathbb{R}^{380}$ , see eq (16).

### 4.4 Local Model Network of the single-hole orifice

The implemented LOLIMOT algorithm uses the input output data, the stopping criteria of the upper limit of a maximum bias error and a maximum number of iteration as input arguments for the systematic and heuristic building of the Neuro-Fuzzy based Local Model Network, see figure 12. The outputs of the algorithm are the resulting Local Model Network and corresponding validity functions. This Local Model Network contains  $M$  local models, which are depicted by the  $M$  number of neurons. Where each  $i^{th}$  local model has a regime characterised by the corresponding validity function  $\phi_i$ , see eq (4).

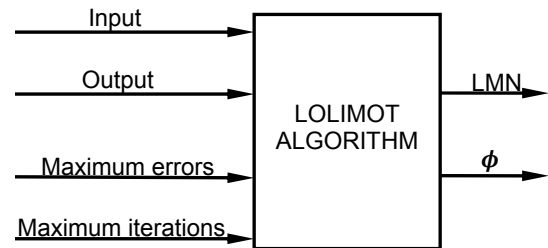


Fig 12 Developing the LMNs

This LMN is the final model for the single-hole orifice which can be used to successfully predict the outputs  $\hat{y}$  at any new evaluating points, see figure 13.

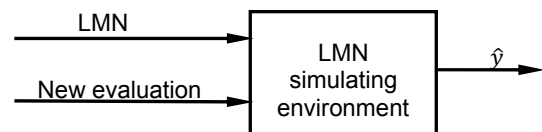


Fig 13 Predicting the outputs

It is important to note that every empirical modelling process faces a bias-variance dilemma [10, 19]. During the implementation of the LOLIMOT algorithm, less number of iteration results in the lower number of parameters that correspond to a higher value of the bias error but a smaller variance error. Similarly the higher the number of iterations the lower will be the bias error but the higher will be the variance error. Since, a low variance value indicates a higher extrapolation capability [10, 19], so, it is important to select a maximum allowed bias error, as this will automatically ensure a minimum possible variance error.

The maximum acceptable bias error can be selected by incorporating the maximum allowed deviation in a particular sound power level at any frequency. The maximum allowed deviation corresponds to the maximum variation in the sound power level before any noticeable change in hearing. Psycho-acoustically, the noticeable change in the sound perception is felt with an at-least 3 dB change in the sound pressure level [20]. So by allowing the uncertainty of 3 dB for each element in the predicted output vector ( $\hat{y} \in \mathbb{R}^{380}$ ), a suitable initial guess for the maximum allowable weighted sum of the square of the errors, see eq(6), has been obtained as 3420, i.e.  $(3)^2 \times 380$ . So by defining the stopping criteria of the maximum weighted squared error as 3420 and initializing the maximum number of iterations as an arbitrary big number, one may run the LOLIMOT algorithm to result in the minimum reasonable number of Local Models required to build an acceptably accurate model.

In this regard, the implemented LOLIMOT algorithm has been run and it was found that after two iterations the criteria of acceptable bias error has been met. The resulting model has been further simplified by using a certain assumption, discussed in section 5. The new assumption helped in achieving the acceptable result after running the algorithm for one iteration only.

## 5 Results

Two series of experiments have been conducted at different times. Both of the experiments were conducted with different operators, different types sound measuring sensors (a free field microphone with diffuse field correction, and a diffuse field microphone), two different impedance convertors, etc. Mean of the overall experimental data has been calculated and it has been found out that most of the experimental data are not deviating, from the mean of the data, by more than a psychological threshold of 3 dB (see figure 14), i.e. a human mind cannot distinguish a noticeable change if the deviation is less than 3 dB [20]. In addition the histogram of the difference, see figure 15, suggest that the difference is normally distributed which indicates that the difference can be taken as random and there exist no bias error. The standard deviation of the error has been found to be  $\sigma = 1.08$ . This indicates a z-score of 2.76 for the

threshold of 3 dB and it can be confidently stated, by using the standard z-score table, that there exists a probability of 99.70 % that the experimental data will not deviate more than is 3 dB. So the mean of the data reasonably represents the reproducibility of the experiments and can be effectively and confidently be considered for the modelling purpose. Although there are in total five readings that are above 3 dB, but they represent a probability of 0.3 % for any such future deviations. In addition, the maximum value that has reached is 3.5 dB, which is psychologically near to the 3 dB and hence can comfortably be ignored.

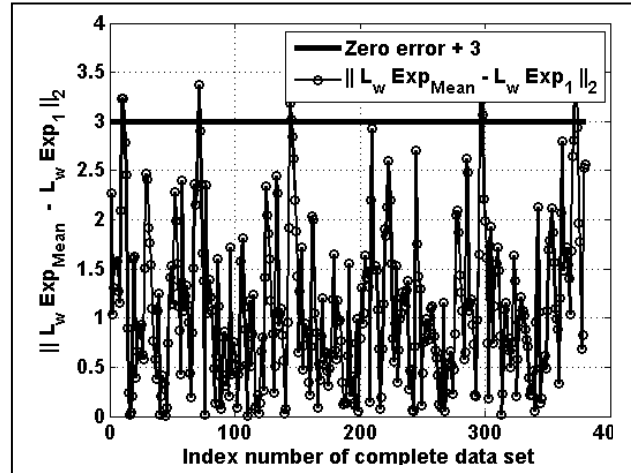


**Fig 14** Absolute error of the data: As there are two sets of experimental data so a difference of one data set from the mean is a mirror image of another, i.e.  $x_1 - \frac{x_1+x_2}{2} = -\left[x_2 - \left(\frac{x_1+x_2}{2}\right)\right]$ .

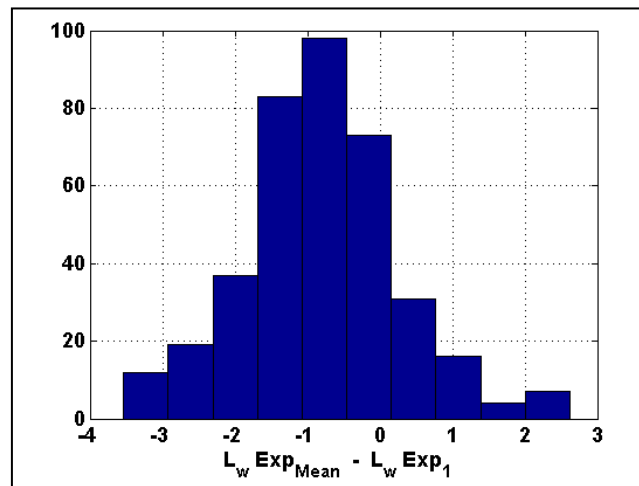


**Fig 15** Histogram of the error

### 5.1 An orifice model: based on two local models

The Neuro-Fuzzy model structure, see eq(5) and figure 7, has been heuristically finalized by implementing the LOLIMOT algorithm, see figure 9. In this regard, the

observed input, i.e.  $opPoints \in \mathbb{R}^{380 \times 3}$ , and output data, i.e.  $y \in \mathbb{R}^{380}$ , were deployed (figure 12 and 13) to result the predicted output, i.e.  $\hat{y} = PCDN \in \mathbb{R}^{380}$ . Finally, the Neuro-Fuzzy based local model network for the predicted output

$$PCDN = (w_{11}\beta + w_{12}R_e + w_{13}kD^{0.15} + w_{10})\phi_1 + (w_{21}\beta + w_{22}R_e + w_{23}kD^{0.15} + w_{20})\phi_2 \quad (18)$$

is obtained. It constitutes two Local Models, where the estimated parameters, i.e.  $w_1, w_2, \phi_1$  and  $\phi_2$  are shown in table 2.

Table 2: Parameters of the LMN with two Local Models

Parameters of the LMN		
Neuron 1	$w_1$	$w_{11} = -51.468$
		$w_{12} = 3.676 \times 10^{-4}$
		$w_{13} = -155.719$
		$w_{10} = 28.131$
	$c_1$	$c_{11} = 0.575$
		$c_{12} = 7.65 \times 10^4$
		$c_{13} = 0.849$
	$\phi_1$	$\sigma_{11} = 0.129$
		$\sigma_{12} = 1.749e \times 10^4$
		$\sigma_{13} = 0.0996$
Neuron 2	$w_2$	$w_{21} = -62.397$
		$w_{22} = 3.658 \times 10^{-4}$
		$w_{23} = -97.764$
		$w_{20} = -24.112$
		$c_2$
$c_{22} = c_{12}$		
$c_{23} = 1.152$		
$\phi_2$	$\sigma_{21} = \sigma_{11}$	
	$\sigma_{22} = \sigma_{12}$	
	$\sigma_{23} = \sigma_{13}$	

### 5.1.1 Residual analyses

For residual analyses, Perrin [19] suggests that two objective functions

$$CR1(\%) = 100 \left[ 1 - \frac{\sum_{i=1}^n (y_i - \hat{y}_i)^2}{\sum_{i=1}^n (y_i - \bar{y})^2} \right] \quad (19)$$

and

$$CR2(\%) = 100 \left[ 1 - \frac{\sum_{i=1}^n (\sqrt{y_i} - \sqrt{\hat{y}_i})^2}{\sum_{i=1}^n (\sqrt{y_i} - \sqrt{\bar{y}})^2} \right] \quad (20)$$

should be used for the assessment of the calibration and the training of the model, where  $y$ ,  $\hat{y}$  and  $\bar{y}$  are the measured, simulated and mean measured outputs, respectively. For a final assessment of a model and for the validation, there is not a single criterion as single criterion may be incomplete [14]. Perrins [19] recommends the criteria

$$CR3(\%) = 100 \left[ 1 - \frac{\sum_{i=1}^n |y_i - \hat{y}|}{\sum_{i=1}^n |y_i - \bar{y}|} \right] \quad (21)$$

and

$$CR4(\%) = 100 \left[ 1 - \left| \frac{\sqrt{\frac{\sum_{i=1}^n \hat{y}_i}{\sum_{i=1}^n y_i}}}{\sqrt{\frac{\sum_{i=1}^n y_i}{\sum_{i=1}^n \hat{y}_i}}} \right| \right] \quad (22)$$

for the complete assessment of the model in terms of the forecast and the validation, which are based on a mean absolute model error and a mean cumulative error, respectively [19].

The results of the residual analyses for the orifice model in eq (18), are shown in table 3. The values depict that up to which percentage the model predicts and validates the measurements.

Table 3: Residual analysis for the orifice model constituting two LMs

Model type	Analysis type	Value %
<i>PCDN</i>	<i>CR1</i>	99.155
	<i>CR2</i>	99.281
	<i>CR3</i>	92.202
	<i>CR4</i>	99.999
<i>L<sub>w</sub></i>	<i>CR1</i>	95.044
	<i>CR2</i>	93.451
	<i>CR3</i>	80.368
	<i>CR4</i>	99.999

Table 3 clearly shows that the empirical model is well calibrated, trained and validated. In addition, the model can also be used with a sufficient reliability for the forecast, at least for the same dynamic and geometric similarities.

The plots for the predicted outputs  $\hat{y}$ , see eq(18), obtained from the newly found LMN that constitutes two Local Models are shown in figures 18 – 20. Each figure represents the simulated and experimental results for a particular orifice, whereas each sub-figure shows the result for a particular fluid condition in that orifice. Each sub figure shows two dotted lines and a solid line, which represents the upper and lower acceptable bound for the predicted output and the experimentally measured output, respectively. One can see that the predicted plot is acceptably inside the  $\pm 3$  dB bound of the experimental mean for the *PCDN*. The figures clearly suggest that the newly found LMN is acceptably predicting the measured results. For a comfortable viewing, some of the results, i.e. results for three out of the five different orifices, are shown. In addition, figures 21 – 23, shows the predicted sound power level by using eq(11). Again it is evident

that the model is effective for the prediction of the sound power level  $L_w$ .

## 5.2 2<sup>nd</sup> orifice model: based on a single local model

One important point to notice is that for low Reynolds numbers, the sound power level, see figures 21 – 23, corresponding to the last two Helmholtz number (corresponds to the frequencies of 16 kHz and 20 kHz) increases in a non-linear way and hence cause the LOLIMOT algorithm to further partition the input along the dimension of the Helmholtz number. A further simplification can be made to the model by ignoring this nonlinearity and limiting the analysis to the frequencies band below 16 kHz. This can be supported on the basis of the observation, see figure 21 – 23, that the sound power levels at the frequencies higher than 16 kHz are too low to significantly contributes the overall sound power levels. In addition, psychoacoustically, a human ear is less sensitive in terms of recognizing the change in power levels at such high frequencies, [20]. So the experimental data has been trimmed (last two entries in each spectrum has been ignored) to cope with the new assumption and again checked for its suitability from statistics point of view.

Similar to the previous non-trimmed data, figure 16 clearly indicates that the most of the newly trimmed data is well within the 3 dB from the mean of the data. Similarly the histogram of the absolute error for the new data, see figure 17, suggest that the difference is again normally distributed and so the difference is random and there exist no bias error. The standard deviation of the error has been found to be  $\sigma = 0.958$ . This indicates a z-score of 3.129 for the threshold of 3 dB and, again by using the z-score tables, it can be confidently stated that there is a probability of 99.91 % that the experimental data will not deviate more than 3 dB from the mean. So the inclusion of the new assumption does not alter the effectiveness of using the trimmed data and the confidence on the reliability of the new trimmed data has been ensured for the modelling purpose. Similar to the previous form of the data, there are in total five readings that are above 3 dB, but, this time, they represent even a lower probability of 0.09 % for any future deviation more than 3 dB. In addition, the maximum value that reached 3.5 dB, which is psychologically near to the 3 dB and hence can once again be ignored comfortably.

With this assumption the algorithm has been run again and resulted in even simpler model (only one local model), which indicates a better variance error as the number of parameters are less. The new form of the resulting model

$$PCDN = w_{11}\beta + w_{12}R_e + w_{13}kD^{0.15} + w_{10} \quad (23)$$

shows a single neuron based model and table 4 shows the parameters for the single Local Model based LMN. As there is only one Local Model, the validity function is a unity, i.e.  $\phi_1 = 1$ , and the parameter vector  $w_1$  is shown in table 4.

Table 4: Parameters of the LMN with one Local Model

Parameters of the LMN		
Neuron 1	$w_1$	$w_{11} = -55.897$
		$w_{12} = 3.807 \times 10^{-4}$
		$w_{13} = -141.399$
		$w_{10} = 18.135$

The corresponding residual analyses are shown in table 5. It is important to note that the new Local Model Network, based on one local model, still possess a reasonable forecasting capability and so it can be utilized for the case where the prediction horizon for Helmholtz number is up to reduce to 3.6. In addition, Figures 24 – 26 and figures 27 – 29 show that an acceptable accuracy along with a less complexity can be achieved for the prediction of both the acoustic quantities, i.e. power coefficient based dimensionless number and sound power level.

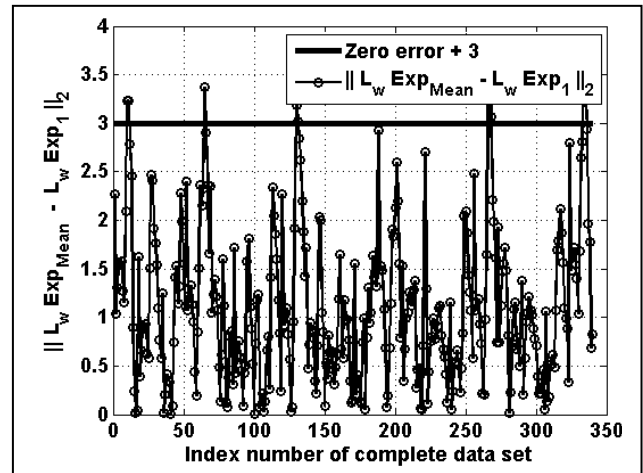


Fig 16 Absolute error of the data for kD up to 3.6

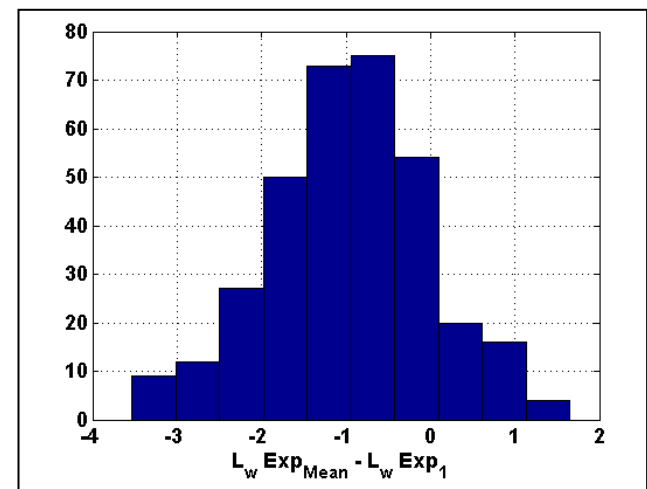


Fig 17 Histogram of the error for kD up to 3.6

Table 5: Residual analysis for the model constituting a LM when the last two frequency bands were ignored for simplification

Model type	Analysis type	Value %
<i>PCDN</i>	<i>CR1</i>	98.904
	<i>CR2</i>	98.934
	<i>CR3</i>	90.244
	<i>CR4</i>	99.999
<i>L<sub>w</sub></i>	<i>CR1</i>	94.495
	<i>CR2</i>	93.785
	<i>CR3</i>	77.442
	<i>CR4</i>	99.999

## 6 Conclusions

For the design of air-distribution system in future aircrafts, an analytical tool has been implemented for the systematic development of an empirical model that allows the prediction of aeroacoustic noise. It is an alternative to the current modelling approaches, since it is efficient and effective and based on a synergic combination of a fuzzy system and an artificial neural network. The resulting Neuro-Fuzzy based local model network combines the interpretability of Fuzzy systems and the quantitative capability of an artificial neural network.

As a representative example, a component of an air-distribution system, namely a single-hole orifice has been considered and modelled for its aeroacoustic prediction. A new power coefficient based dimensionless number has been introduced which makes the modelling process easier. Two model structures based on the Neuro-Fuzzy method were heuristically developed by using the LOLIMOT algorithm whose parameters were identified by using the linear least square method. The final models use the fluid and geometric variables and predict the sound spectrum as an output which is successfully validated by using the residual analyses. The results show that there is a good agreement between the experimental and simulated results, i.e. for both the spectrum of the power coefficient based number and the sound power level.

The models effectively predict the aeroacoustic behaviour of an orifice. The same approach may be applied to other parts of an air-distribution system, e.g. branched duct, curved pipes, air outlet, etc. The models will then be connected in a modular way to simulate the complete aeroacoustic behaviour of an air-distribution system. Moreover, the same approach can be applied on other engineering problems where an empirical model is required.

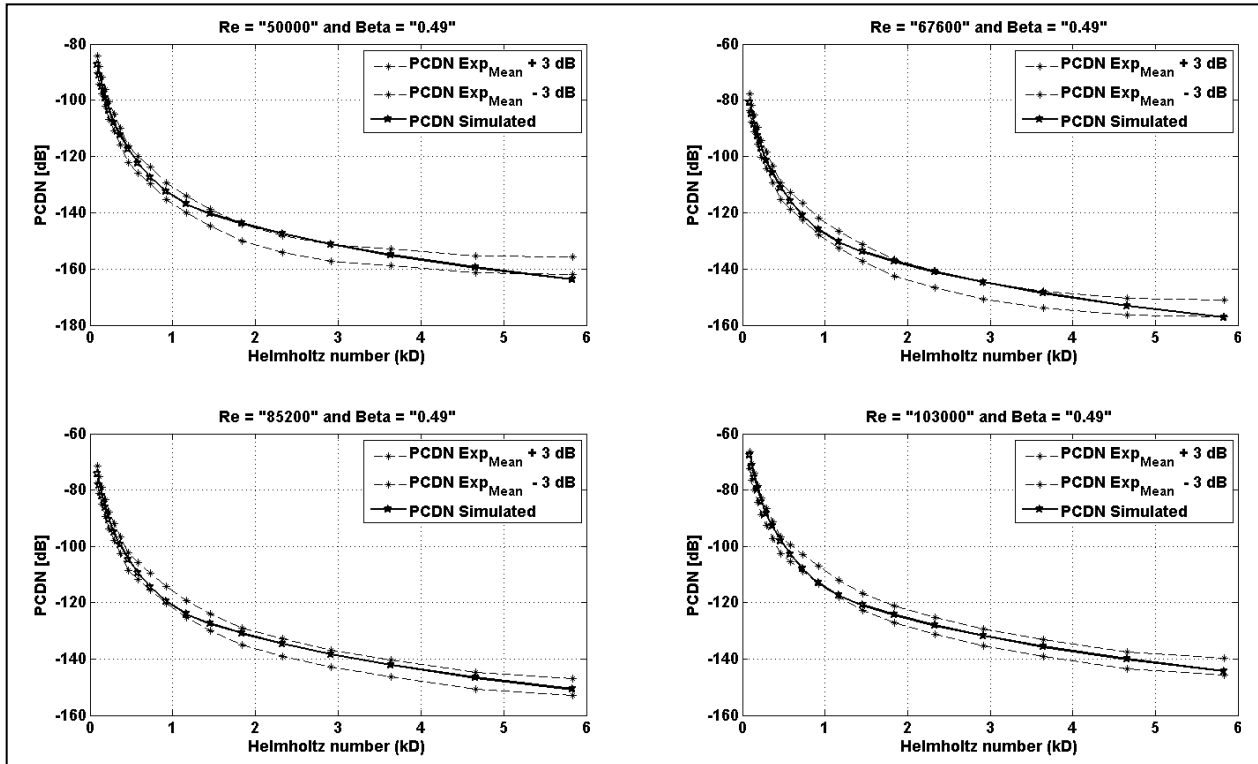


Fig 18 Predicted and measured PCDN for orifice of diameter ratio 0.49 with kD up to 5.8

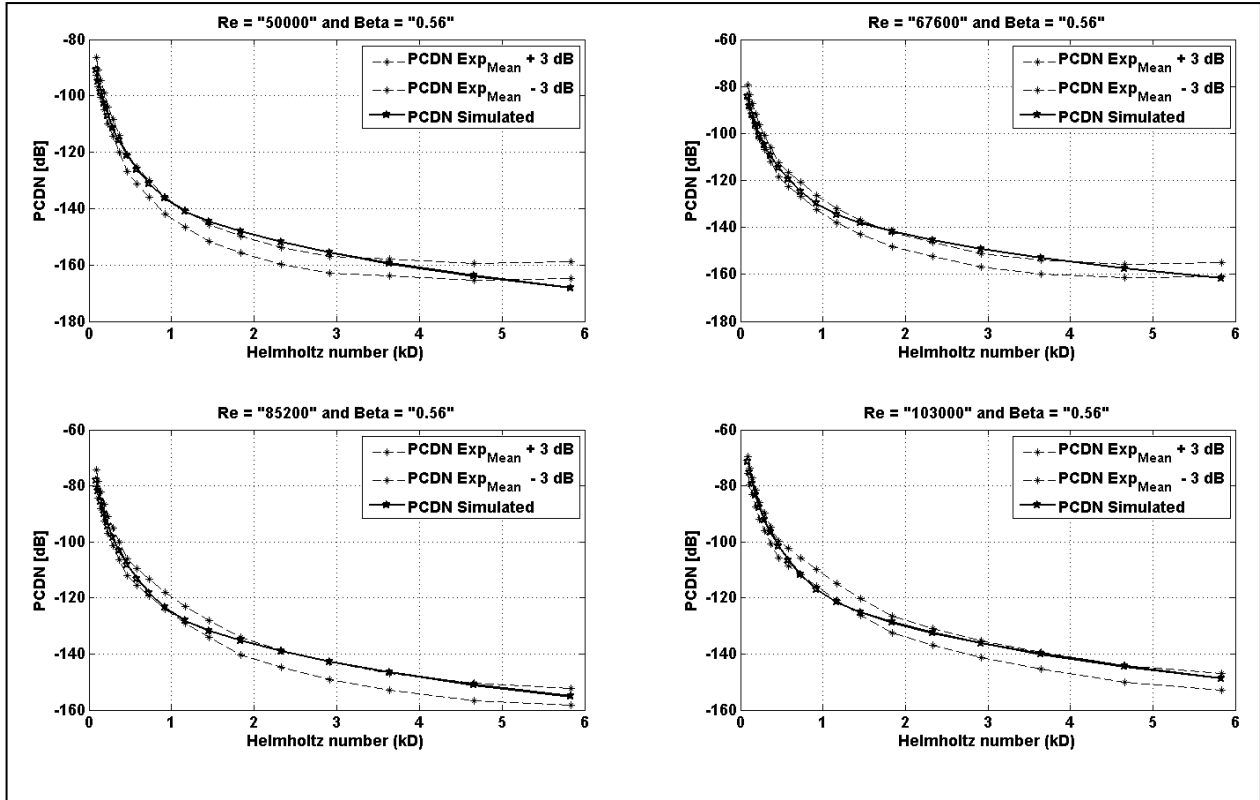


Fig 19 Predicted and measured PCDN for orifice of diameter ratio 0.56 with kD up to 5.8

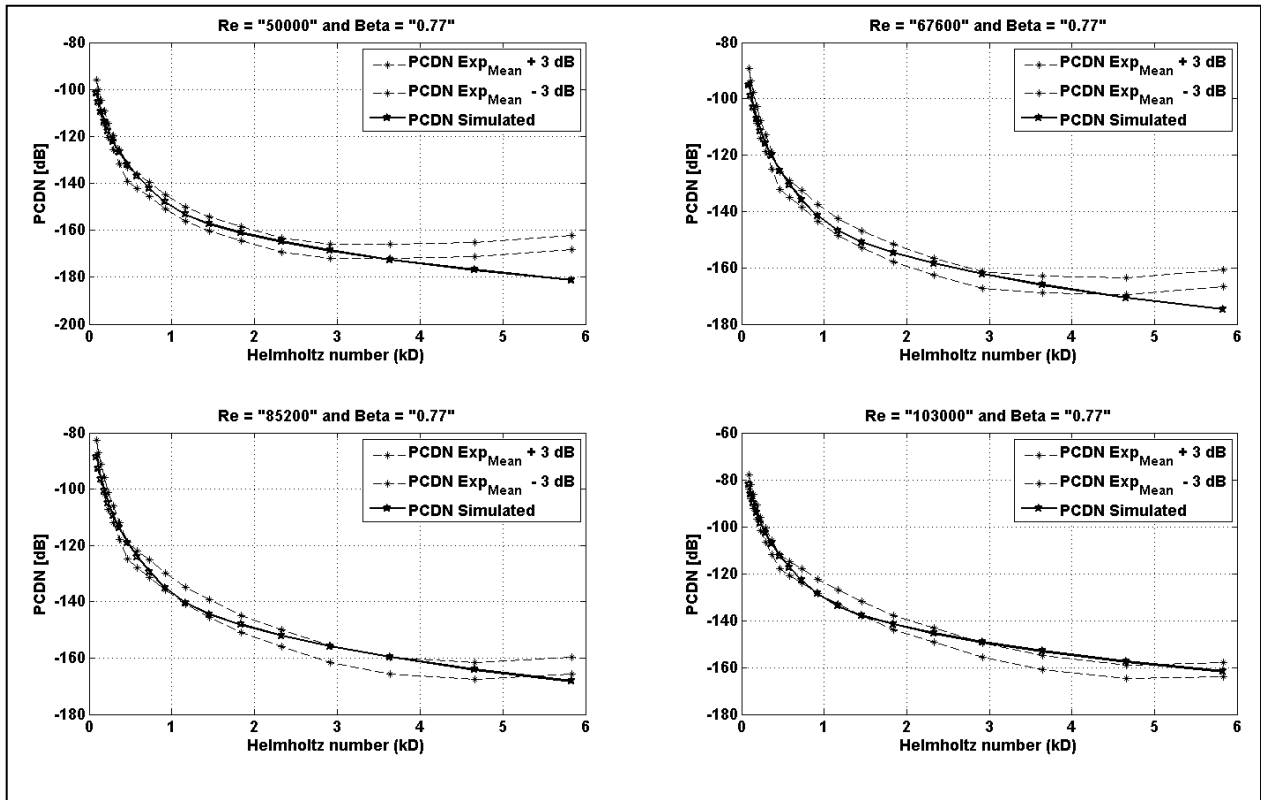


Fig 20 Predicted and measured PCDN for orifice of diameter ratio 0.77 with kD up to 5.8

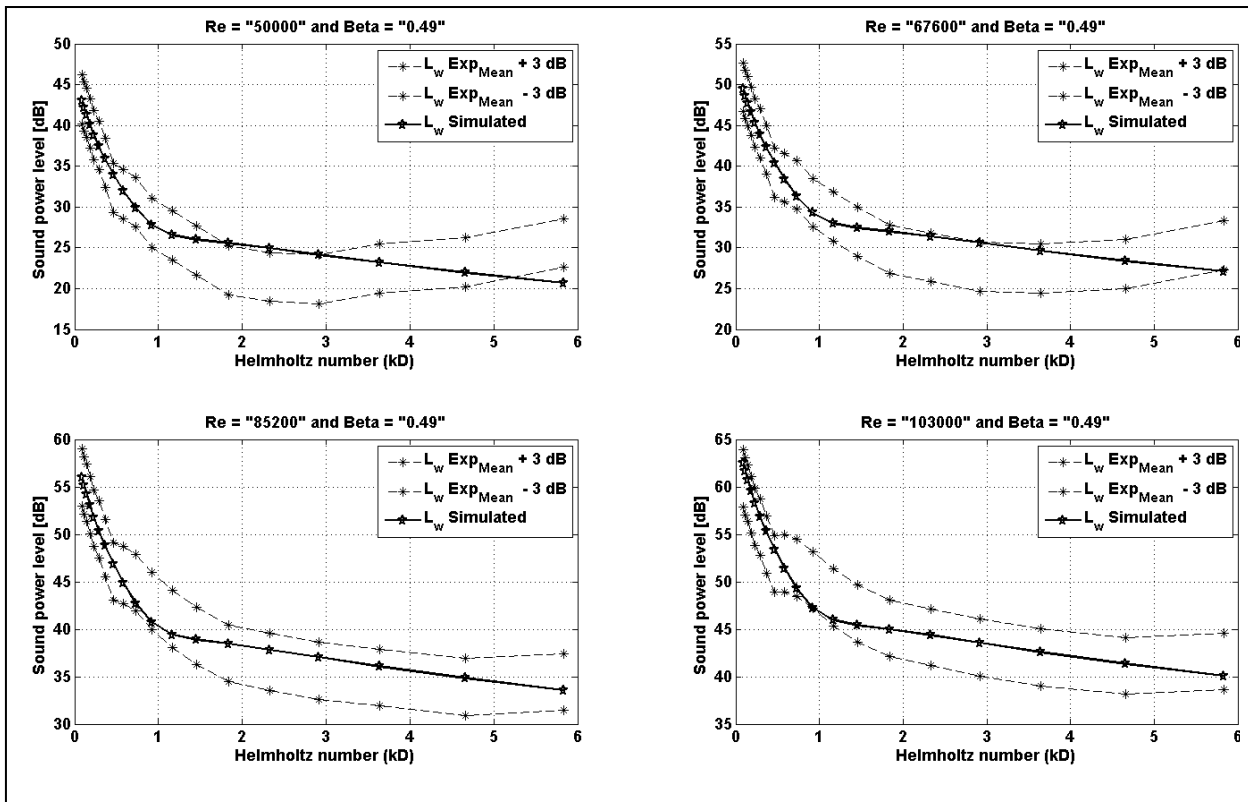


Fig 21 Predicted and measured sound power level for orifice of diameter ratio 0.49 with kD up to 5.8

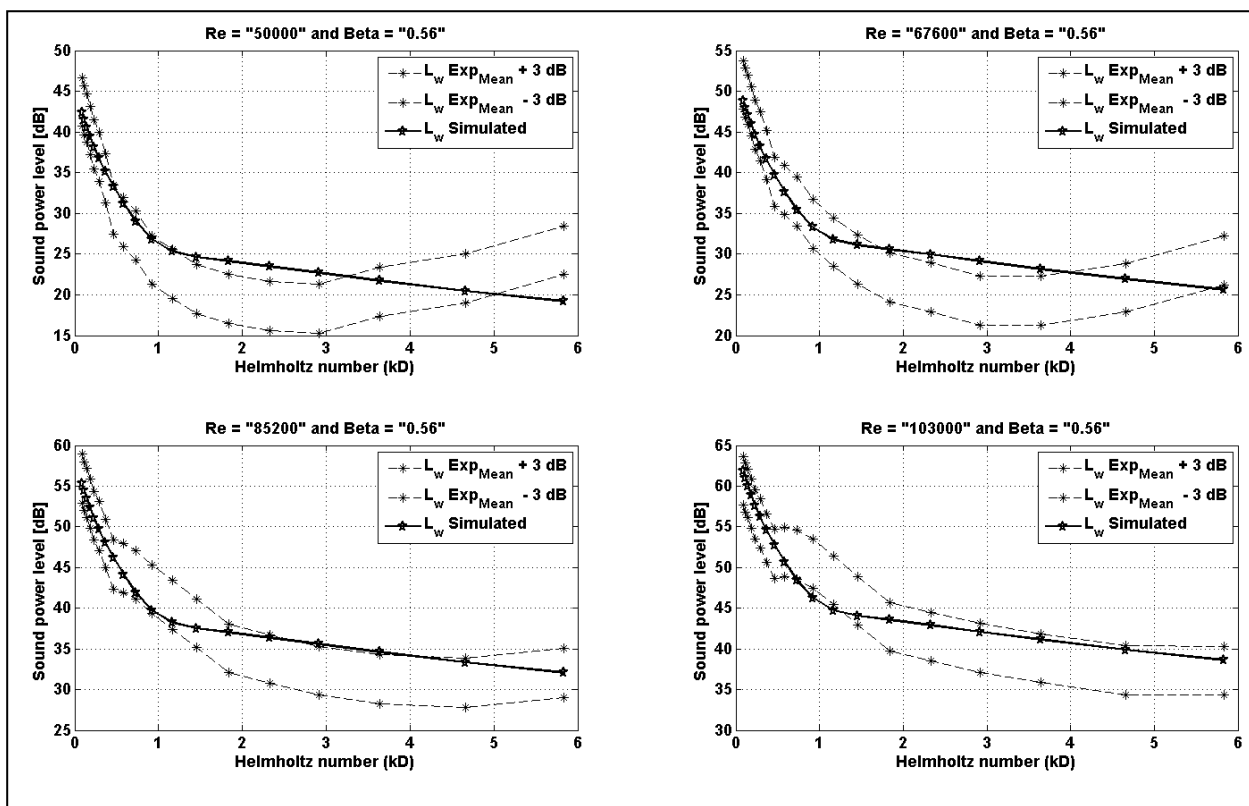


Fig 22 Predicted and measured sound power level for orifice of diameter ratio 0.56 with kD up to 5.8

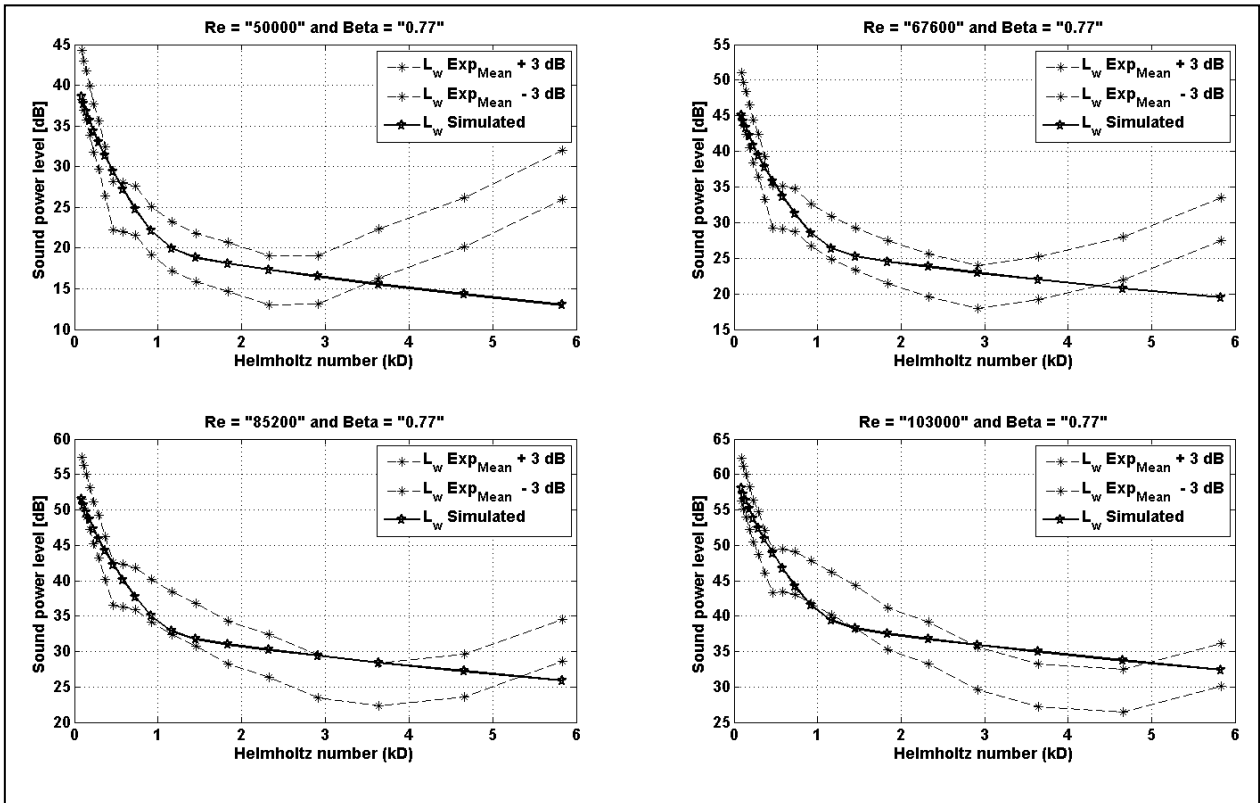


Fig 23 Predicted and measured sound power level for orifice of diameter ratio 0.77 with kD up to 5.8

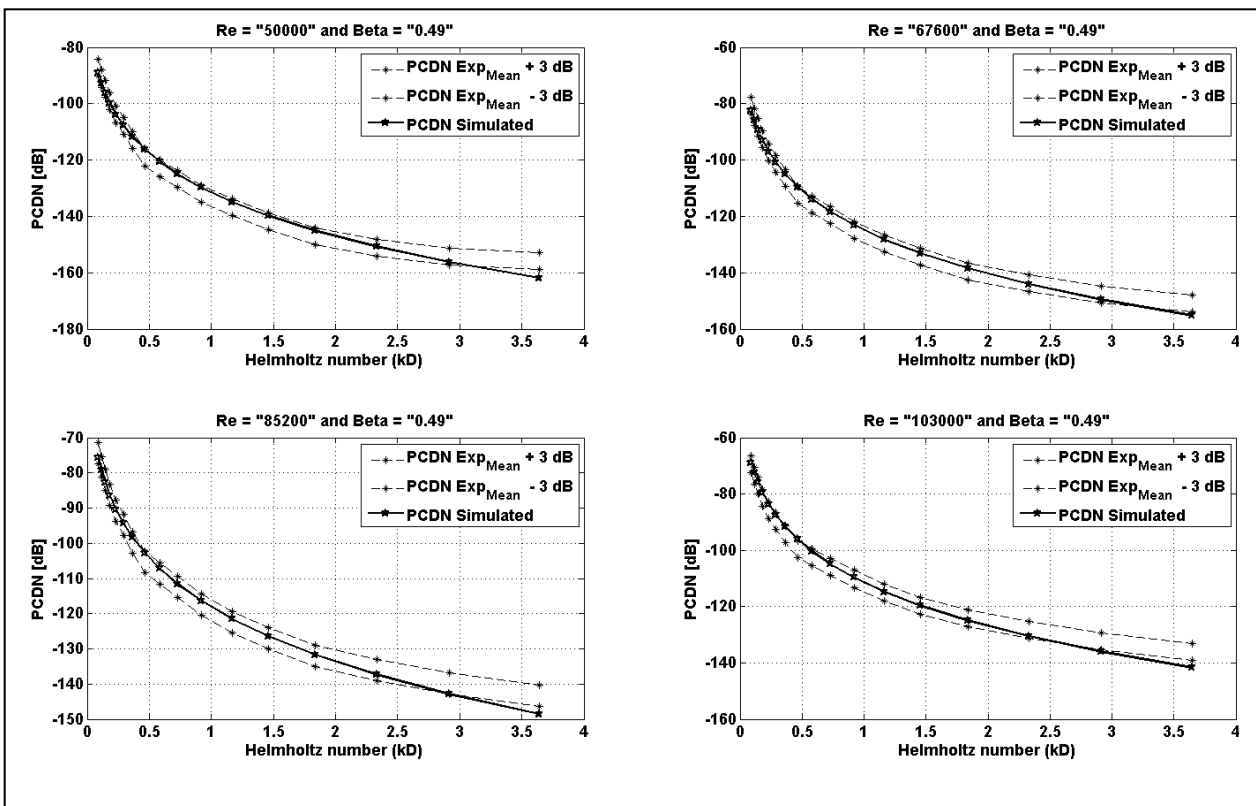


Fig 24 Predicted and measured PCDN for orifice of diameter ratio 0.49 with kD up to 3.6

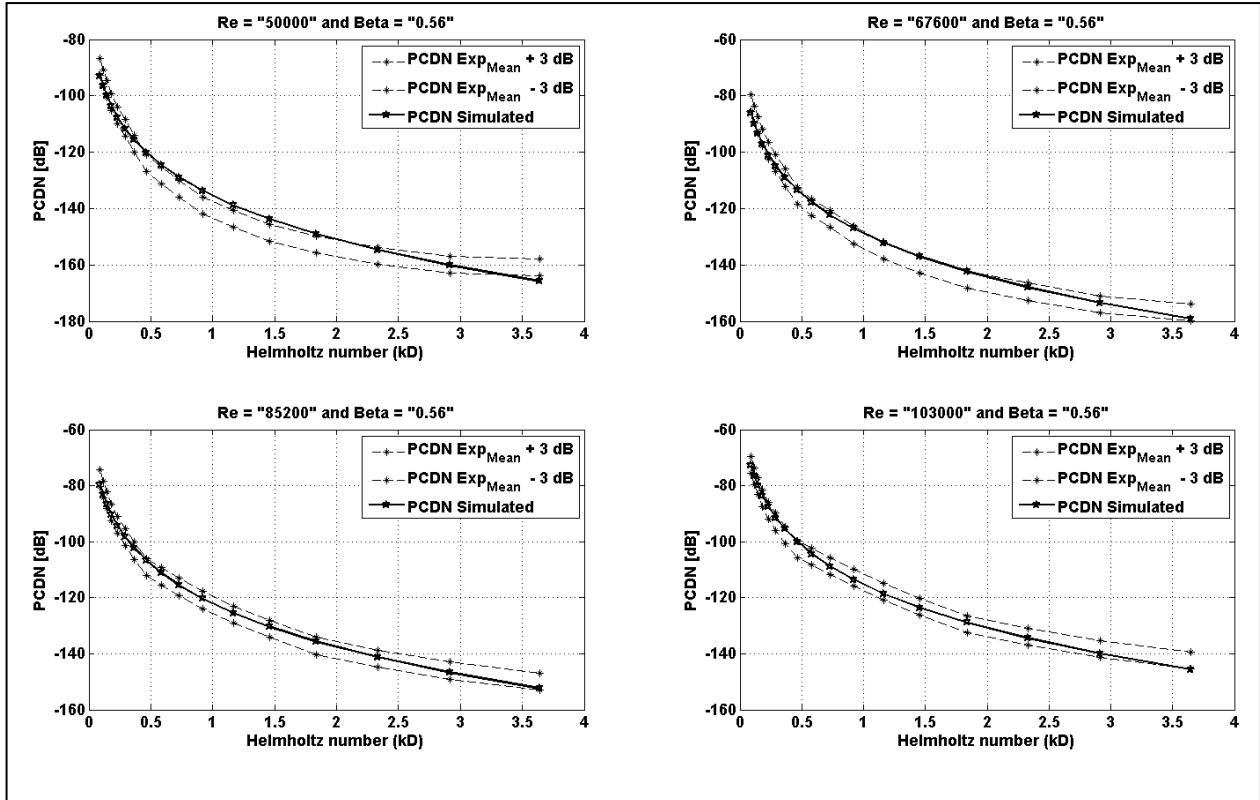


Fig 25 Predicted and measured PCDN for orifice of diameter ratio 0.56 with kD up to 3.6

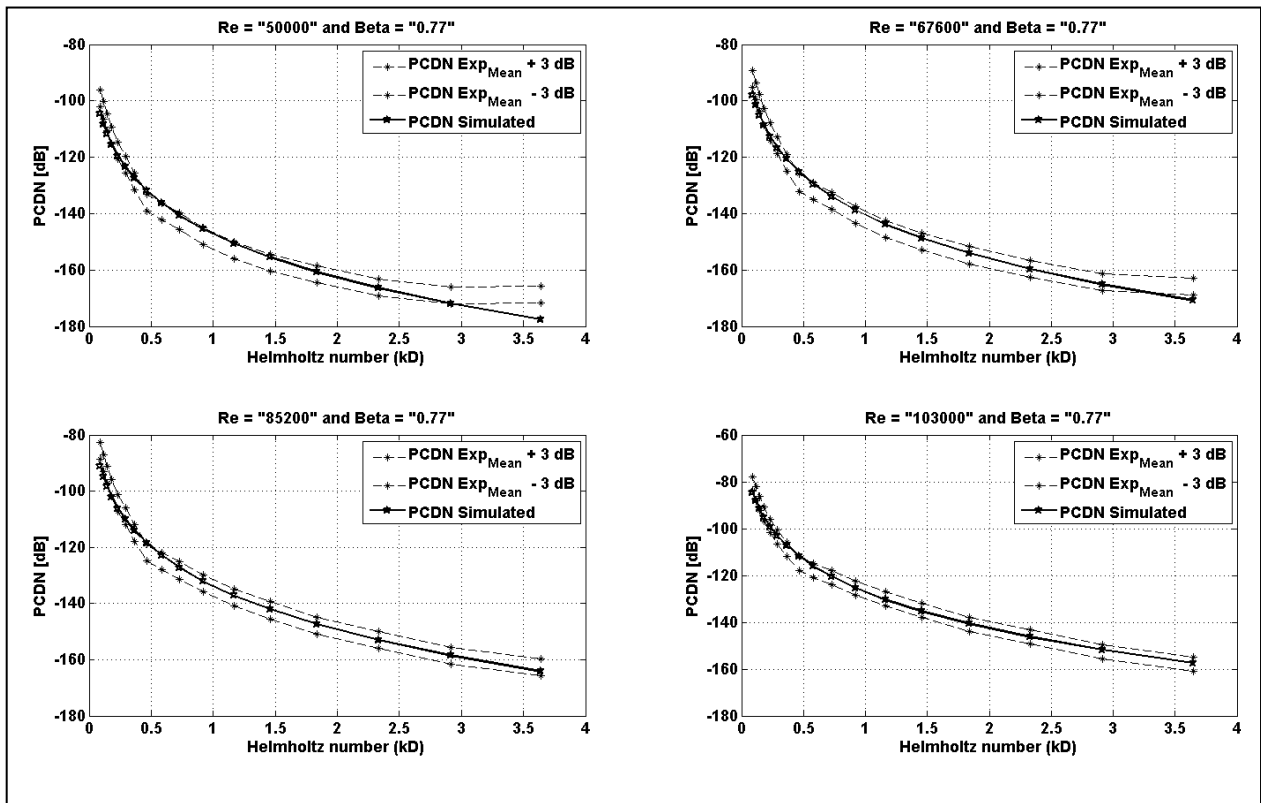


Fig 26 Predicted and measured PCDN for orifice of diameter ratio 0.77 with kD up to 3.6

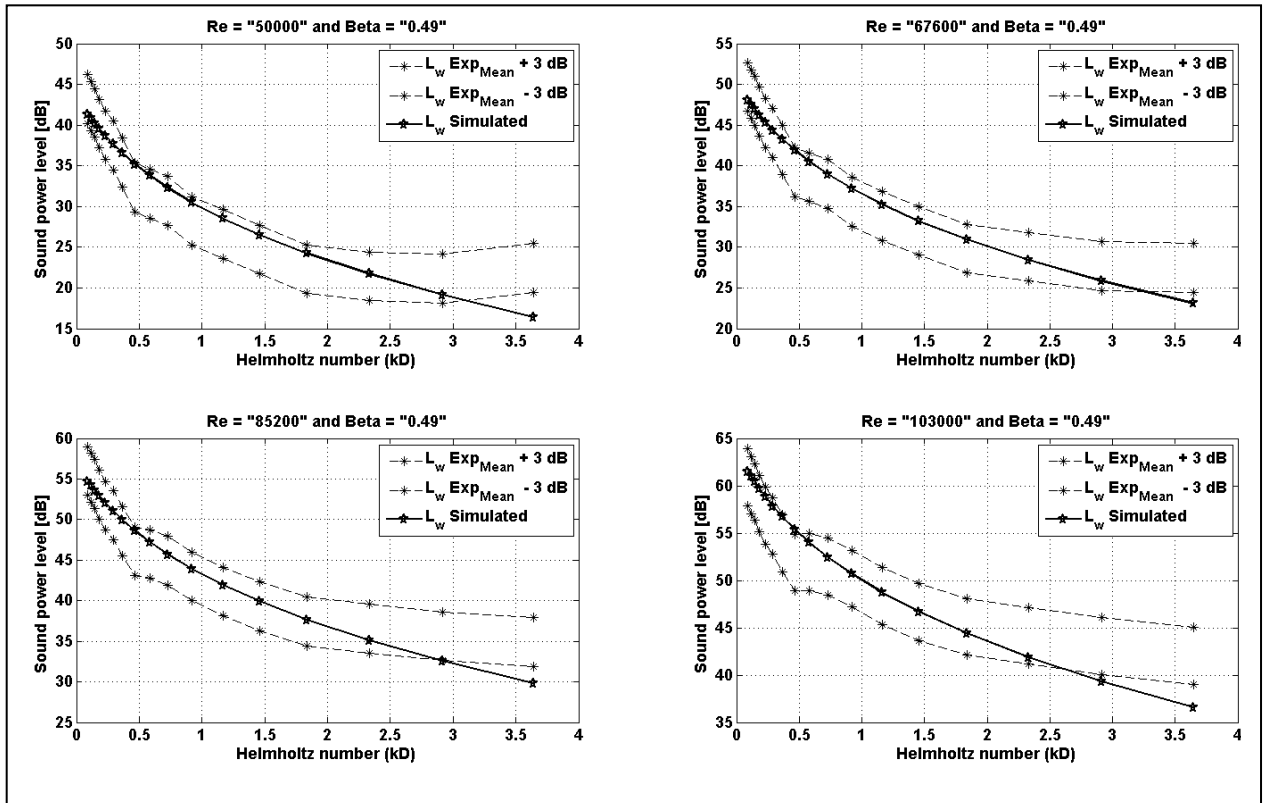


Fig 27 Predicted and measured sound power level for orifice of diameter ratio 0.49 with kD up to 3.6

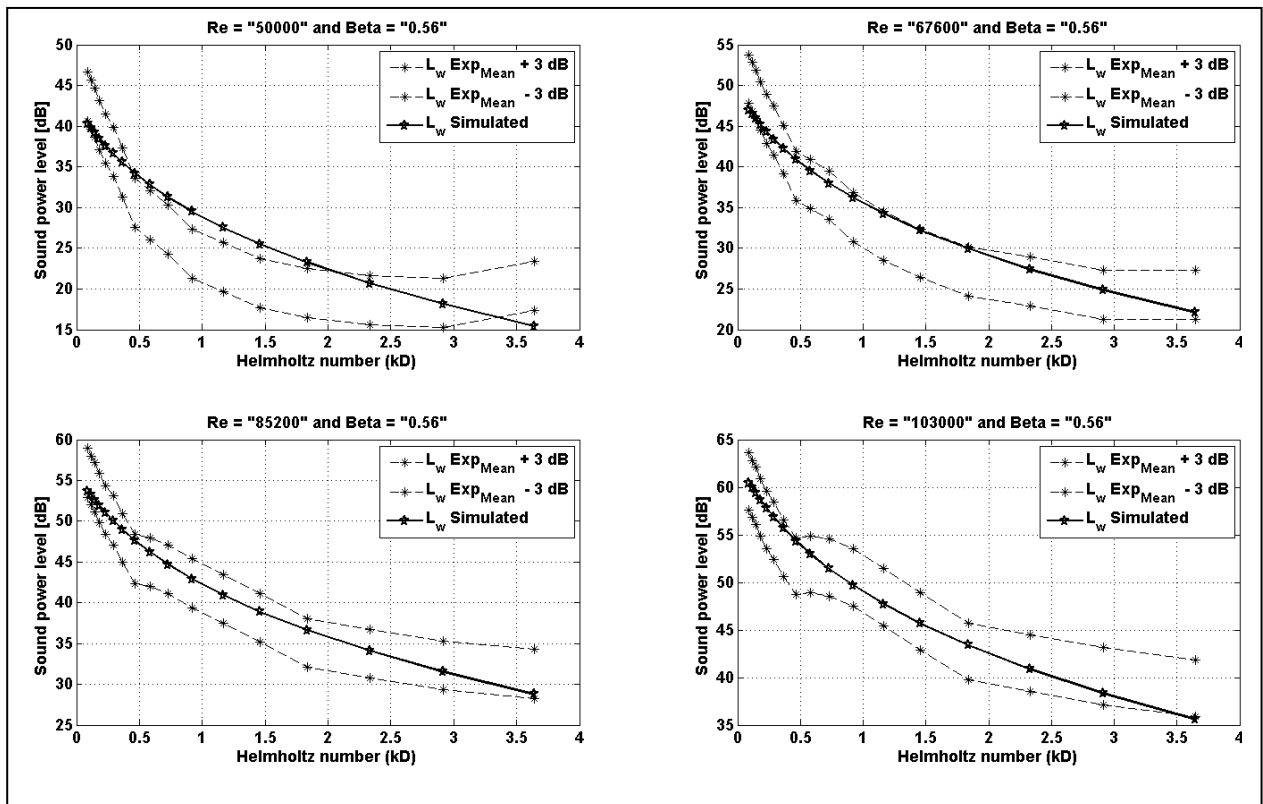


Fig 28 Predicted and measured sound power level for orifice of diameter ratio 0.56 with kD up to 3.6

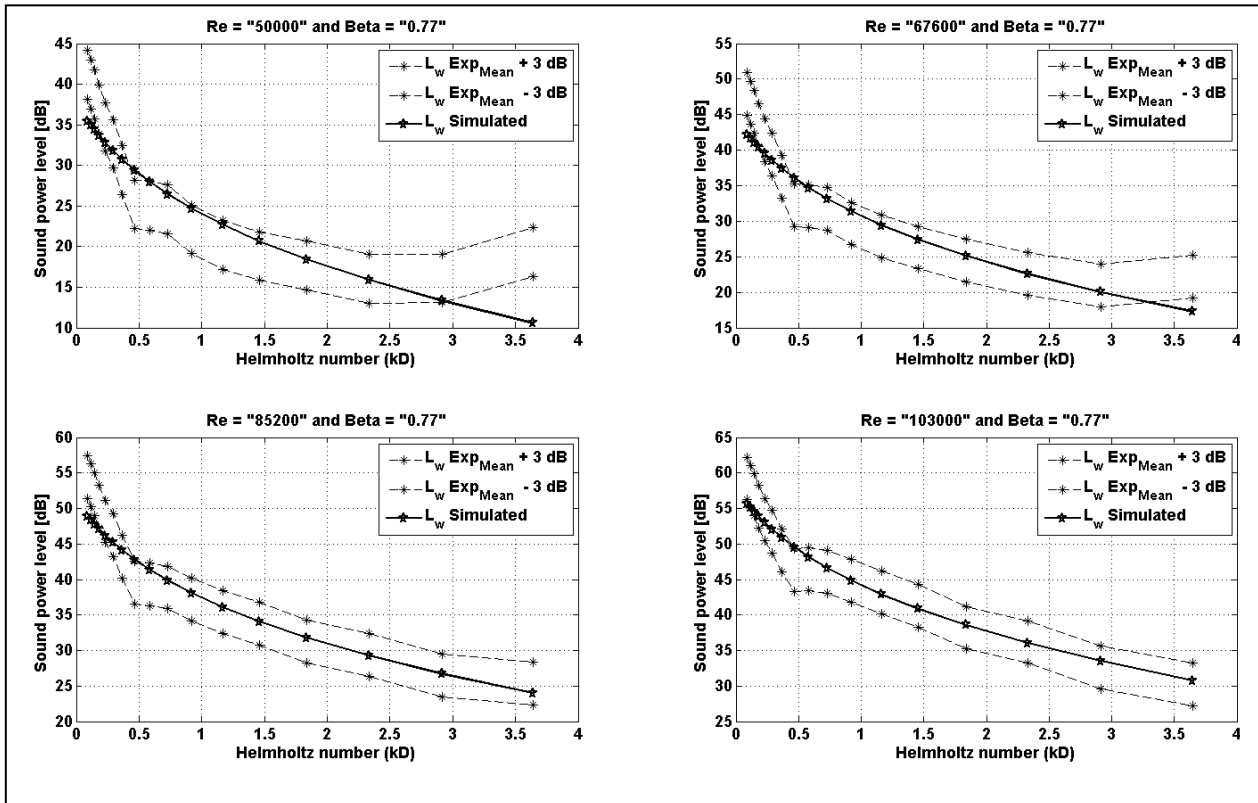


Fig 29 Predicted and measured sound power level for orifice of diameter ratio 0.77 with kD up to 3.6

## 7 Acknowledgment

The financial support by Behörde für Wirtschaft, Verkehr und Innovation BWVI (the authority for business, transportation and innovation) Hamburg Germany through the project HH 131 B is greatly acknowledged. In addition, the feedbacks of Prof. Dr.-Ing. Wolfgang Gleine along with the assistance of Mr. Muhammad Saqib Shahzad are very much appreciated.

## 8 Appendix

### 8.1 Biological neural network

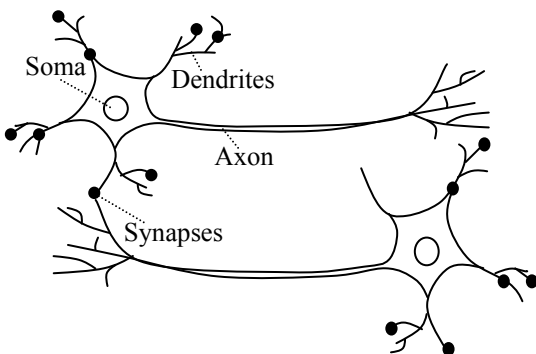


Fig 30 Two interconnected biological neurons. A biological neuron consists of a Soma, Dendrites, an Axon and Synapses. All the incoming signals, generated by

some external stimuli, enter the logical part of the neuron, called Soma, through Dendrites. The Soma adds all the input signals and logically realizes them. If the summed signal surpasses the threshold then the Soma converts the signal into an activation signal in the form of a pulse sequence, which propagates along an Axon, as an output and may enter into another neuron via Synapses. Finally, a complex combination of different neurons provides a brain an outstanding pattern recognition and concept making capability.

### 8.2 A Gaussian function: A type of a radial basis function

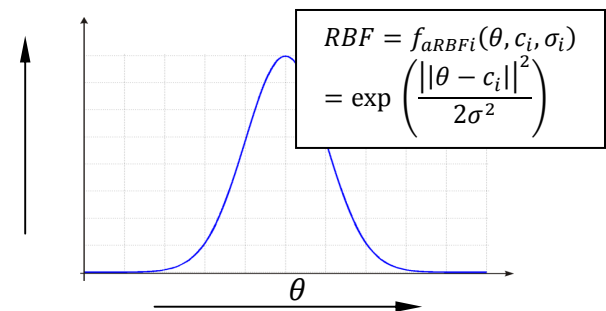


Fig 31 Gaussian function an example of a radial basis function

### 8.3 Activation Functions

Different activation function,  $f_a(\cdot)$  are shown in figure 41.

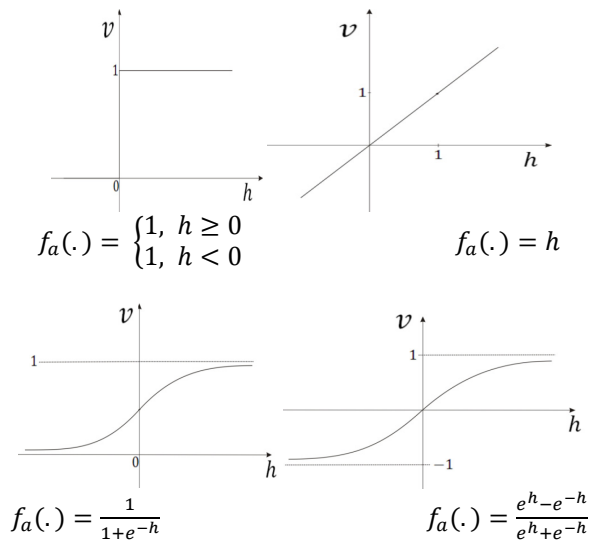


Fig 32 Different activation function

## 9 Reference

- [1] Facts sheet: Public health preparedness, International Air Transport Association (IATA), [http://www.iata.org/pressroom/facts\\_figures/factsheets/Pages/health.aspx](http://www.iata.org/pressroom/facts_figures/factsheets/Pages/health.aspx), updated June (2012).
- [2] Wang, M.; Freund, J. B.; Igle, S. K.: Computational prediction of flow-generated sound, *The Annu. Rev. of Fluid Mech.* **38**, 483 – 512, (2006).
- [3] Fedorchenko, A. T.: On some fundamental flaws in present aeroacoustic theory, *J. of Sound. and Vib.* **232**(4), 719 – 782, (2000).
- [4] White, F. M.: *Fluid mechanics*, McGraw-Hill, 4<sup>th</sup> Edition.
- [5] Tam, C. K. W.: Computational aeroacoustics: An overview of computational challenges and applications, *Int. J. of Comput. Fluid Dyn.* **18**, 547 – 567, (2004).
- [6] Bokhar, S. F., von Estorff, O., Grunau, E., Stoob, M, Gleine, W.: Development of an experimental setup for the investigation of aeroacoustics effects inside aircraft air-distribution system, In: *Deutscher Luft- und Raumfahrtkongress (German Aerospace Congress)*, 405 – 411, ISBN: 978-3-932182-68-5.
- [7] Gregorcic, G.; Lightbody, G.: Local model network identification with Gaussian process, *IEEE Trans. on Neural Net.* **18**(5), 1404 – 1423, (2007).
- [8] Bänfer, O., Nelles, O., Kainz, J., Beer, J.: Local Model Networks with Modified Parabolic Membership Function, *IEEE* (2009), doi:10.1109/AICI.2009.477.
- [9] Babuska, R., Verbruggen, H.: Neuro-fuzzy methods for nonlinear system identification, *Annu. Rev. in Control.* (2003) doi:10.1016/S1367-5788(03)00009-9
- [10] Nelles, O.: *Non-linear system identification*, Springer-Verlag Berlin Heidelberg, (2001).
- [11] Murray-Smith, R.; Johansen, T. A.: *Multiple model approaches to modelling and control*, Taylor & Francis, (1997).
- [12] Garcia-Nieto, S., Martinez, M., Blasco, X., Sanchis, J.: Nonlinear predictive control based on local model networks for air management in diesel engines, *Control. Eng. Pract.* **16**, 1399 – 1413, (2008).
- [13] Fink, A., Töpfer, S., Isermann, R.: Nonlinear model-based control with local linear neuro-fuzzy models, *Arch. of Appl. Mech.* **72** (2003), doi:10.1007/SO 0419-002-0264-3.
- [14] Takagi, T.; Sugeno, M.: Fuzzy identification of systems and its application to modelling and control, *IEEE Trans. on Syst. Man, and Cybern.* **15**(1), 116 – 132, (1985).
- [15] Szirtes, T.: *Applied dimensional analysis and modelling*, 2<sup>nd</sup> edition, Butterworth-Heinemann, (1997).
- [16] Manas, K. D.; Anindya, D.: The matrix method: A powerful technique in dimensional analysis, *The J. of Frankl. Inst.* **321**, 233 – 240, (1986).
- [17] Cobb, G. W.: *Introduction to Design and Analysis of Experiments*, Springer, (1997).
- [18] Lazik, Z. R.: *Design of Experiments in Chemical Engineering: A Practical Guide*, Wiley, (2004).
- [19] Perrin, C.; Michel, C.; Andreassian, V.: Does a large number of parameters enhance model performance? Comparative assessment of common catchment model structure on 429 catchments, *J. of Hydrol.* **242**, 275 – 301, (2001).
- [20] Bruel & Kjaer Sound & Vibration Measurement A/S, *Environmental Noise*, (2001).
- [21] *Neural Network Toolbox™ User's Guide for MatLab R2012a*, The Mathworks, Inc. (2012).
- [22] *Fuzzy Logic Toolbox™ User's Guide for MatLab R2012a*, The Mathworks, Inc. (2012).